HAL
open science

Systematic uncertainties in air shower measurements from high-energy hadronic interaction models

R.D. Parsons, C. Bleve, S.S. Ostapchenko, J. Knapp

To cite this version:

R.D. Parsons, C. Bleve, S.S. Ostapchenko, J. Knapp. Systematic uncertainties in air shower measurements from high-energy hadronic interaction models. Astroparticle Physics, 2011, 34 (11), pp.832. 10.1016/j.astropartphys.2011.02.007 . hal-00741513

HAL Id: hal-00741513

https://hal.science/hal-00741513

Submitted on 13 Oct 2012

HAL is a multi-disciplinary open access archive for the deposit and dissemination of scientific research documents, whether they are published or not. The documents may come from teaching and research institutions in France or abroad, or from public or private research centers.

L'archive ouverte pluridisciplinaire **HAL**, est destinée au dépôt et à la diffusion de documents scientifiques de niveau recherche, publiés ou non, émanant des établissements d'enseignement et de recherche français ou étrangers, des laboratoires publics ou privés.

Accepted Manuscript

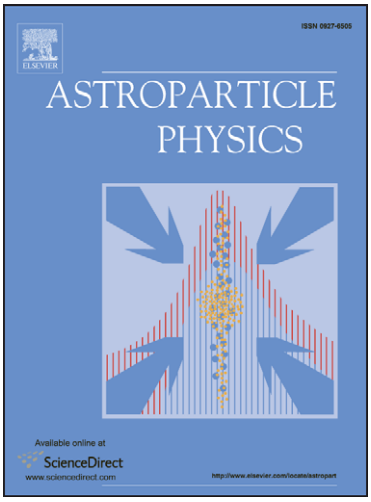

Systematic uncertainties in air shower measurements from high-energy hadronic interaction models

R.D. Parsons, C. Bleve, S.S. Ostapchenko, J. Knapp

PII: S0927-6505(11)00053-3
DOI: 10.1016/j.astropartphys.2011.02.007
Reference: ASTPHY 1582

To appear in: *Astroparticle Physics*

Received Date: 4 January 2011
Revised Date: 17 February 2011
Accepted Date: 21 February 2011

Please cite this article as: R.D. Parsons, C. Bleve, S.S. Ostapchenko, J. Knapp, Systematic uncertainties in air shower measurements from high-energy hadronic interaction models, *Astroparticle Physics* (2011), doi: 10.1016/j.astropartphys.2011.02.007

This is a PDF file of an unedited manuscript that has been accepted for publication. As a service to our customers we are providing this early version of the manuscript. The manuscript will undergo copyediting, typesetting, and review of the resulting proof before it is published in its final form. Please note that during the production process errors may be discovered which could affect the content, and all legal disclaimers that apply to the journal pertain.

ACCEPTED MANUSCRIPT

Systematic uncertainties in air shower measurements from high-energy hadronic interaction models

R.D. Parsons[a], C. Bleve[b], S.S. Ostapchenko[c,d], J. Knapp[a]

[a] *School of Physics and Astronomy, University of Leeds, Leeds, LS2 9JT, UK*
[b] *Dept. of Physics, Bergische Universität Wuppertal, 42119 Wuppertal, Germany*
[c] *Institutt for Fysikk, NTNU, 7491 Trondheim, Norway*
[d] *D.V. Skobeltsyn Institute of Nuclear Physics, Moscow State University, 119992 Moscow, Russia*

Abstract

Hadronic interaction models at cosmic ray (CR) energies are inherently uncertain due to the lack of a fundamental theoretical description of soft hadronic and nuclear interactions and the large extrapolation required from collider energies to the range of the most energetic cosmic rays observed $> 10^{20}$ eV). Model uncertainties are evaluated within the QGSJET-II model, by varying some of the crucial parameters in the limits allowed by collider data, and between QGSJET-II and other models commonly used in air shower simulations. The crucial parameters relate to hard processes, string fragmentation, diffraction and baryon production. Results on inelastic cross sections, on secondary particle production and on the properties of air showers measured by ground detectors from energies of 10^{12} to 10^{19} eV are presented.

1. Introduction

Direct measurements of the primary cosmic rays (CR) with energies $\geq 10^{12}$ eV are generally difficult due to their exceedingly low flux. Instead, their properties are reconstructed from the shape and particle content of the extensive air showers (EAS) they produce in the atmosphere. The reconstruction is based on numerical models of the air shower development. As there is currently no reliable fundamental theory describing soft hadronic interactions at high energies, large systematic uncertainties limit the precision of the results. Most current hadronic interaction models use Gribov-Regge theory [1] of multi-Pomeron exchange between nucleons as the basis for the treatment of high-energy, soft interactions, which are prevalent in air showers. Perturbative quantum chromodynamics (pQCD) can describe hard interactions with high $p_\perp$, which are rare in cosmic ray interactions, but become more important at higher energies. In addition, diffractive interactions, collisions of nuclei, and interactions and decays of all possible secondary particles at energies from MeV to beyond 10^{20} eV are needed for a complete simulation of an air shower. The generalisation from nucleon-nucleon to hadron-nucleus and nucleus-nucleus collisions is usually performed via the Glauber-Gribov formalism [2, 3], taking into account inelastic screening and low mass diffraction effects. Particle tracking and electromagnetic interactions are straight forward to simulate. The major problem is the seamless and coherent combination of the different parts of hadronic models. Different numerical codes implement the same theoretical ideas in different ways, with approximate agreement at lower energies where collider data are used for tuning, but diverging in the region where extrapolations are required, e.g. to ultra high energies, or to very forward emission directions.

An important aspect of the analysis of experimental data, is the estimation of systematic uncertainties of air shower observables, due to imperfections of the current interaction models. The sensitivity of the simulated EAS observables to various extrapolations of characteristics of hadronic interactions, such as the inelastic cross section, the multiplicity of secondary particles or the relative energy loss of the leading (most energetic) hadrons, towards very high energies has been recently investigated in [4]. While that study is certainly very illustrative, the variations considered can hardly be achieved in realistic models, without being in contradiction with available accelerator data or with fundamental principles of the quantum field theory. For example, one of the options investigated in Ref. [4] assumed the inelastic hadron-nucleus cross section to rise asymptotically as $\ln^3 s$ (s being the square of the c.m. energy of the collision), thus violating the unitarity bound.

In the present work a different strategy is chosen. We investigate the potential spread in the high energy extrapolations of hadronic interaction characteristics and the related uncertainties of air shower simulations within a particular model framework. We quantify the uncertainties of the model, by varying some crucial model parameters within the limits allowed by accelerator data. In this way, we also take into

ACCEPTED MANUSCRIPT

account the correlations between different interaction characteristics. For example, constraints on the rise of the total proton-proton cross section with energy come also from the data on the pseudorapidity (η) density of secondary charged hadrons. The main question addressed here are how uncertain predictions can be (within a particular model) and if the uncertainties can cover the differences between currently available Monte Carlo generators of hadronic interactions.

For our study we chose the latest version of the QGSJET model, QGSJET-II-3 ([5], released in 2006), because QGSJET describes quite well a large set of experimental air shower data at energies from 10^{12} to 10^{20} eV. Additionally, QGSJET-II provides a microscopic treatment of nonlinear interaction effects in hadronic and nuclear collisions, described by Pomeron-Pomeron interaction diagrams, which become very important at very high energies. We construct a number of alternative parameter sets (options 2 to 6) for the model and compare the results obtained with the standard QGSJET-II (option 1) and with two models often used in air shower physics, namely SIBYLL 2.1 [6] and EPOS 1.99 [7]. While the original SIBYLL was based on the "minijet" idea, ascribing the energy evolution of the interaction cross section and particle production solely to the contribution of hard processes (minijet emission), the actual model version is rather similar to the Gribov-Regge-type models. A crucial difference between QGSJET-II and SIBYLL 2.1 is that parton saturation effects in SIBYLL are modelled by means of an energy-dependent cutoff for the minijet production. EPOS employs a phenomenological approach for nonlinear interaction effects, while addressing an important problem of energy-momentum correlations between multiple scattering processes at the amplitude level [8]. EPOS has a significantly larger number of adjustable parameters than QGSJET-II, but a substantially larger set of accelerator data has been used for its calibration. The distinctive feature of EPOS is the enhanced production of baryons, which leads to more energy in the muonic component of showers [9]. The standard versions of all these models are available in the framework of the latest CORSIKA air shower simulation package [10].

2. Parameter Variations in QGSJET-II

Among the crucial parameters responsible for the high energy extrapolation of the model are those related to inelastic diffraction, the relative contributions of soft and hard processes, and the distribution of energy-momentum between secondary particles. To investigate the corresponding allowed parameter range, five versions (option 2-6) of the QGSJET-II model have been created, with varying parameter settings, which are tuned to reproduce (within experimental accuracy) *the same set* of accelerator data as used for the original model calibration. The new data obtained at the Large Hadron Collider (LHC) have not yet been used in the analysis. The effects of the parameter variations are then investigated for both single interactions and air showers as a whole. Option 1 corresponds to the standard parameter settings of QGSJET-II (see Tab. 1).

Diffractive interactions are very important for the shower development, as they transport the primary energy efficiently through the atmosphere. Both, projectile and target nucleons can undergo low-mass diffraction excitation. The latter is treated in QGSJET-II in the framework of the Good-Walker-like multi-channel eikonal approach [11, 12]: A hadron is represented by a superposition of a number of elastic scattering eigenstates which undergo different absorption, depending on their relative strength λ_i for the interaction. For the 2-component scheme realised in QGSJET-II, the ratio λ_1/λ_2 defines thus the strength of diffraction, which rises for more asymmetric superposition (larger λ_1/λ_2) and disappears for $\lambda_1 = \lambda_2$. In addition, a stronger diffraction implies also stronger inelastic screening effects which reduce the predicted total and inelastic cross sections. The parameters are varied in two different ways to increase the proportion of diffractive events and influence the rise with energy of total inelastic hadron-hadron and hadron-nucleus cross sections. In the default version of QGSJET-II (option 1) the corresponding ratios are $\frac{\lambda_1}{\lambda_2}(p) = 4$ for protons and $\frac{\lambda_1}{\lambda_2} = 4.7$ and 5.7 for pions and kaons respectively. The corresponding low

option	diffraction		Q_0^2	BJM	SE
	$\frac{\lambda_1}{\lambda_2}(p)$	$\frac{\lambda_1}{\lambda_2}(\pi)$	(GeV^2)		
1 (std)	4	4.7	2.5	on	0.5
2	**7**	**9**	2.5	on	0.5
3	4	4.7	**4**	on	0.5
4	4	4,7	2.5	**off**	0.5
5	4	4.7	2.5	**off**	**0.7**
6	4	**3**	2.5	on	0.5

Table 1: Parameter settings of six options of QGSJET-II. Option 1 represents the standard settings of QGSJET-II. See text for further explanations.

ACCEPTED MANUSCRIPT

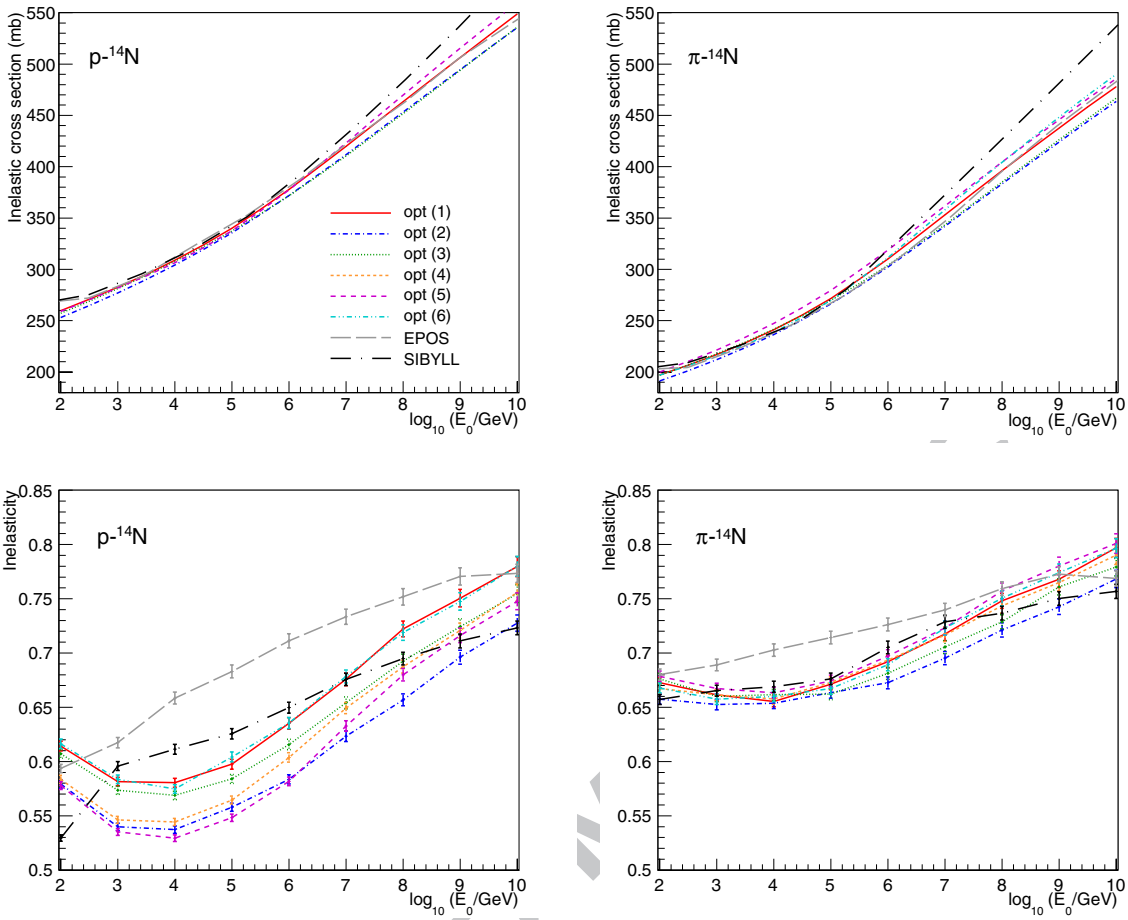

Figure 1: **Top:** Inelastic cross sections for proton-Nitrogen and π-Nitrogen collisions.
Bottom: Inelasticity of p-Nitrogen and π-Nitrogen collisions.

mass diffraction cross section for the incident hadron changes between 0.9 and 1.6 mb for proton-proton and between 1.2 and 1.7 mb for pion-proton interactions in the laboratory energy range of 10^2 to 10^8 GeV. In option 2 we enhance low-mass diffraction by choosing $\frac{\lambda_1}{\lambda_2}(p) = 7$ and $\frac{\lambda_1}{\lambda_2}(\pi) = 9$, $\frac{\lambda_1}{\lambda_2}(K) = 12$, while in option 6 we leave proton diffraction unchanged but decrease diffraction for pions and kaons, $\frac{\lambda_1}{\lambda_2}(\pi, K) = 3$. As an illustration of the discussed modifications, in option 2 the low mass diffraction cross section of the projectile hadron at 10^2 and 10^8 GeV is increased to 1.6 and 3.1 mb, respectively, in pp collisions and to 2.0 and 3.2 mb in πp interactions.

In the Gribov-Regge framework, QGSJET takes into account contributions of both soft and semihard parton cascades. In the latter case, the virtuality (q^2) cutoff Q_0^2 defines the transition from the non-perturbative soft ($|q|^2 < Q_0^2$) to the perturbative hard ($|q|^2 > Q_0^2$) part of the cascade. Additionally, in QGSJET-II the shadowing and saturation effects are accounted for by the soft ($|q|^2 < Q_0^2$) partons. Thus, the performance of the model depends strongly on this cutoff parameter and on the parton distribution functions obtained from deep inelastic scattering. As the semi-hard contribution rapidly increases with energy, one can significantly reduce the rise of the cross sections and the secondary particle production with energy when this cut-off is increased from its default value 2.5 GeV^2 to 4 GeV^2, as done in option 3.

Options 4 and 5 vary the energy-momentum partition between elementary production processes and string fragmentation. In option 4 the "baryon junction" mechanism (BJM) [13], related to di-quark valence quark interactions, is switched off, leading to a slower energy rise of the inelasticity in proton-proton and especially in proton-nucleus collisions. In option 5, in addition the parameter α_q for the momentum distribution ($\sim x^{-\alpha_q}$) of constituent (anti-)quarks - string ends (SE) was modified from the default value 0.5 to 0.7, which also enhances the leading particle effect in high energy interactions.

In addition, with the exception of option 4, which is identical to the default model version apart from the above-discussed modification, for each new parameter set created a re-tuning of other model parameters was performed in order to keep the agreement with accelerator data. The corresponding

ACCEPTED MANUSCRIPT

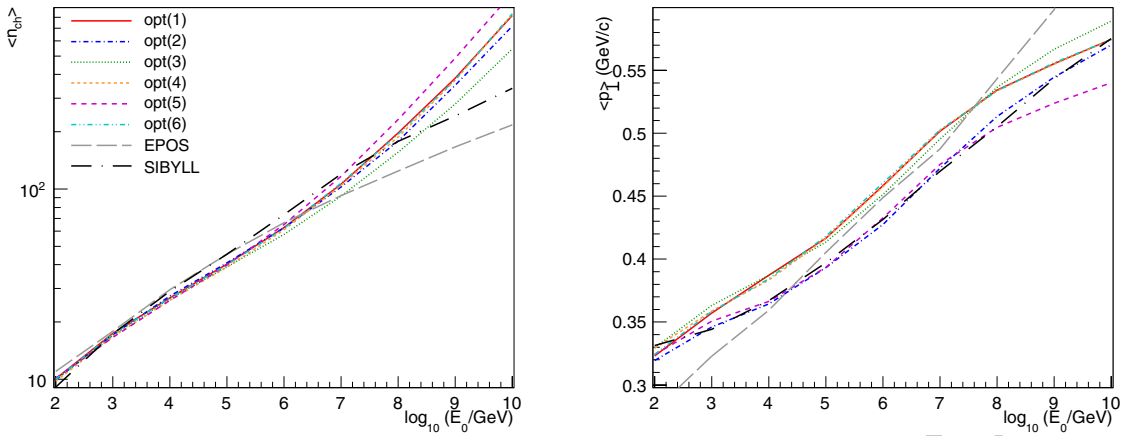

Figure 2: **Left:** Average multiplicity of charged particles and
right: average $p_\perp$ for proton-Nitrogen interactions as function of lab energy.

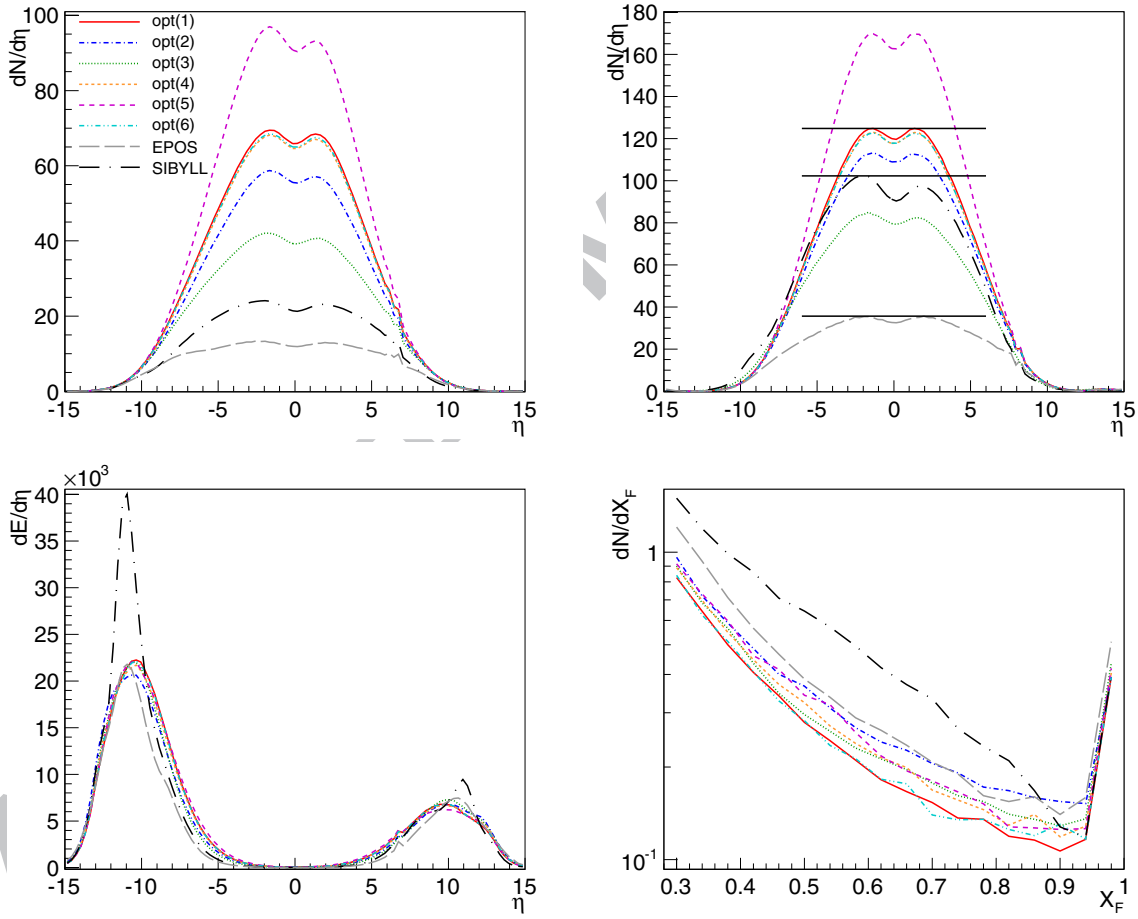

Figure 3: **Top:** $dN/d\eta$ distributions for charged particles from p-Nitrogen (left) and Nitrogen-Nitrogen (right) collisions at $E_{\rm lab} = 10^{19}$ eV. In these plots lines from options 1, 4 and 6 lie on top of one another. **Bottom:** $dE/d\eta$ distributions (left) and Feynman-x distributions (right) for charged particles from p-Nitrogen collisions. All plots are for 10^{19} eV. Colours as for Fig. 2.

changes were minimal for option 6 (weaker diffraction for pions and kaons), which concerned the Pomeron-pion interaction vertex only. For option 5, a significant modification of the string fragmentation procedure was necessary to compensate the decrease of particle multiplicity due to shorter strings. An opposite procedure has been used for option 2, where the particle yield from fragmenting strings was decreased.

ACCEPTED MANUSCRIPT

For options 2, 3, and 5, most of the basic model parameters, like Pomeron intercept and slope, Pomeron-hadron couplings, and parton (quark and gluon) distributions in the Pomeron had to be re-tuned, which was necessary to remain in agreement with the data on total and elastic hadron-proton cross sections, elastic scattering slopes, and on the proton structure function F_2.

The main parameters modified in the different model versions are listed in Tab. 1. While the parameters investigated here are certainly crucial ones, it is not clear whether they are the only ones that matter. The comparison with EPOS shows that there are other mechanisms which can influence significantly the shower properties and consequently affect the interpretation of air shower experiments.

3. Single Interactions

In this section the particle production in individual collisions is investigated. It relates directly to the particle content and shape of showers, and is crucial for energy determination and composition analysis in air shower experiments. Overall, for all options a reasonably good agreement between the available collider data at low energies and the simulations was achieved. The evolution at high energies Fig. 1 shows the inelastic cross sections and the inelasticity of p-Nitrogen and π-Nitrogen collisions as a function of energy, for all the models. The cross sections of the QGSJET variants have similar shapes and the differences between the options are within 10%, even at the highest energies, with the smallest values being obtained for options 2 and 3 (higher diffraction and higher Q_0-cutoff, respectively). EPOS shows a cross section very similar to the QGSJET models, which could be expected as both models are genuinely based on Gribov-Regge theory. However, SIBYLL shows a rounder shape with a much steeper increase at high energies, most likely being related to the adopted parametrisation for the energy-dependent cutoff of minijet production.

The inelasticity is the fraction of energy used for the production of secondary particles, i.e. $1 - E_{\rm lp}/E_{\rm tot}$, where $E_{\rm lp}$ is the energy of the leading baryon for proton collisions and the leading charged meson for pion collisions. The evolution of the inelasticity as function of $E_{\rm lab}$ is shown at the bottom of Fig. 1. These plots show that all QGSJET model variants produce a similarly shaped dependence of inelasticity with energy, with a characteristic minimum around $10^3 - 10^4$ GeV, but some are shifted to lower inelasticity values by up to 0.05. This is also true for the inelasticity of pion-Nitrogen collisions, except that the shifts are much smaller. Both, EPOS and SIBYLL, show significantly different shapes in inelasticity vs. energy, but with similar values as QGSJET at around 10^{12} eV and 10^{19} eV.

Fig. 2 shows the average number of charged particles produced in p-Nitrogen collisions. $\langle n_{\rm ch} \rangle$ is very similar for all the models, up to a lab energy of about 10^{17} eV, where the models start to diverge. At the highest energies the QGSJET variants all produce 2-5$\times$ more secondaries than SIBYLL or EPOS. All models predict a similar average $\mathrm{p}_\perp$ growing with energy, only EPOS gives smaller $\mathrm{p}_\perp$ values below 10^4 GeV and larger ones above 10^8 GeV (see Fig. 2, right).

The large differences in particle numbers can also be seen in the pseudorapidity distributions of charged particles (see Fig. 3). QGSJET produces the largest numbers of secondaries, and there are big differences among its variants. At 10^{19} eV QGSJET option 5 produces almost 50% more, and option 3 only half the number of particles than option 1 in the central region ($\eta \approx 0$). SIBYLL and EPOS are even lower than option 3. Recent measurements at LHC in the central pseudorapidity range indicate indeed that QGSJET-II tends to overestimate the central pseudorapidity density of secondary hadrons (see [14] for a detailed comparison. However, most of these particles are emitted with low energies, compared to the energy of the parent hadron. Although differences can be also seen at larger pseudorapidities, these are of much smaller magnitude than in the centre. While being relevant for calculations of the muon content of air showers, the hadrons in the central rapidity region are of little importance for the longitudinal shower development. The fact that the forward particles are more important can be seen from the distribution of the energy flux ($\mathrm{dE/d}\eta$) vs. pseudorapidity in Fig. 3 bottom, left. In the forward region, where diffractive interactions contribute and where most of the interaction energy is going, all the models are fairly close together. Very little energy emitted in the central region, despite the large number of particles. EPOS shows good agreement with the QGSJet variants. SIBYLL, however, has prominent peaks in $\mathrm{dE/d}\eta$ in the forward and backward regions. Also the Feynman-x distributions show that there is fair agreement between all the models in the very forward region ($x_{\rm F} = p_{\rm L}/p_{\rm max} \geq 0.95$).

The η distributions also allow assessment of the treatment of nuclear interactions in the models, which is important for nuclear composition studies of cosmic rays. As Nitrogen-Nitrogen collisions are perfectly symmetric, also the η distribution should be symmetric. In QGSJET nuclear interactions are modeled as two clouds of nucleons penetrating each other and interacting. As the modeling is done in a symmetric way also the outcome is symmetric. Also EPOS produces a symmetric distribution. SIBYLL models nuclear interactions with the semi-superposition model which treats a nuclear projectile as a

ACCEPTED MANUSCRIPT

superposition of individual nucleons and a nucleus-nucleus collision as a number of independent nucleon-nucleus collisions. This is by construction asymmetric and therefore the Nitrogen-Nitrogen collisions result in asymmetric pseudorapidity distributions. SIBYLL produces $> 4\times$ more particles in Nitrogen-Nitrogen than in p-Nitrogen collisions, while for QGSJET and EPOS this factor is only about 2. Thus, for composition studies based on differences in the muon yield in showers from different nuclei, it is better to rely on QGSJET or EPOS.

The large differences in η between models and the comparison with first collider data at high energies indicate that some aspects of the models are not correct and need adaptation. Although currently there are only few measurements in the relevant forward region and LHC is not yet running at its maximum energy, LHC results, in particular, the results of the LHCf experiment [15] provide already constraints to some of the model parameters. Future measurements of the total proton-proton cross section and of particle production at $\sqrt{s} = 14$ TeV will greatly help to tune the models further.

4. Air Showers

Showers were simulated at energies of 10^{12} eV, 10^{15} eV and 10^{19} eV, i.e. at typical energies relevant to Cherenkov telescopes (such as HESS [16], VERITAS [17] and MAGIC [18]), small air shower arrays (such as KASCADE [19] and LHAASO [20]), and experiments for the highest energies (e.g. the Telescope Array [21] or the Pierre Auger Observatory [22]), respectively. The first interaction point of the primary particle was fixed at typical values for the respective primary energy, to exclude the effect of shower-to-shower fluctuations due to the varying point of first interaction and to concentrate on differences in shower shape. For each energy the average longitudinal development and the lateral distribution of particles at ground level have been determined. Also characteristic observables were evaluated, such as the average values of the atmospheric depth of the shower maximum, $X_{\max}$, the particle number at the shower maximum, $N_{\max}$, the Cherenkov photon lateral distribution at ground level, the electron-to-muon ratio at ground level, the energy that would be released in an Auger-like water Cherenkov detector at 1000 m core distances (S_{1000}) [23] and the time in which the integrated signal grows from 10% to 50%, $t_{1/2}$ [24]. Simulations have been performed for the QGSJET variants as well as for SIBYLL 2.1 and EPOS 1.99 to allow comparisons between the scale of the uncertainties due to parameter variations within a model, and due to model-to-model variations.

4.1. Low Energies (10^{12} eV)

At 10^{12} eV very little variation is found in both the lateral distribution and the longitudinal development, for the QGSJET options, with differences being $\leq 10\%$ for all quantities investigated. This is not surprising as the energy is close to the accelerator energies at which the models have been tuned.

However, as the number of shower particles reaching ground level at this energy is very low, a more appropriate observable is the lateral distribution of Cherenkov photons at ground level. The number of Cherenkov photons relates to the primary energy, but is different for different primaries. Proton

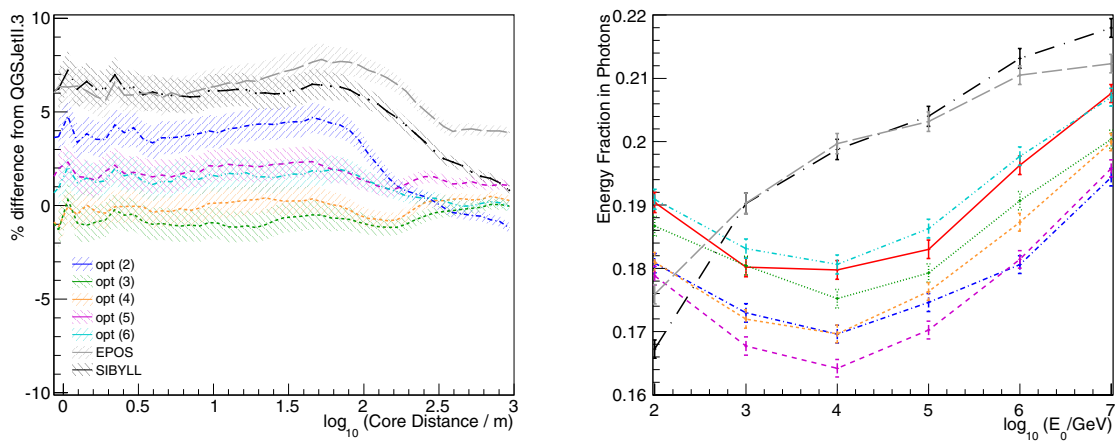

Figure 4: **Left:** Percentage difference of the Cherenkov photon density ρ (for $\lambda = 300$-600 nm) compared to the standard QGSJET-II model (i.e. $\rho_{\rm i}/\rho_{\rm std}) - 1$). Results from 10^4 vertical proton showers of 10^{12} eV. Atmospheric absorption is accounted for. Error bars show statistical errors of the mean values. **Right:** Fraction of total interaction energy emitted in photons as a function of energy ($E_\gamma/E_{\rm tot}$)

ACCEPTED MANUSCRIPT

Model	$N_e(10^3)$	$N_\mu(10^3)$	N_e/N_μ	$X_{\max}$ (g/cm^2)	$N_{\max}(10^3)$
QGSJET-II (1)	208 ± 4	10.3 ± 0.1	20.8 ± 0.4	546 ± 3	566 ± 4
QGSJET-II (2)	219 ± 4	9.4 ± 0.1	24.0 ± 0.5	552 ± 4	577 ± 4
QGSJET-II (3)	211 ± 5	10.3 ± 0.1	21.6 ± 0.8	548 ± 4	571 ± 3
QGSJET-II (4)	203 ± 4	10.1 ± 0.1	21.0 ± 0.5	542 ± 3	574 ± 3
QGSJET-II (5)	204 ± 4	10.3 ± 0.1	20.1 ± 0.4	542 ± 3	567 ± 3
QGSJET-II (6)	195 ± 4	9.8 ± 0.1	20.6 ± 0.5	534 ± 3	579 ± 3
SIBYLL 2.1	201 ± 4	9.4 ± 0.1	22.1 ± 0.5	539 ± 3	571 ± 4
EPOS 1.99	178 ± 3	11.8 ± 0.1	16.3 ± 0.6	528 ± 3	564 ± 4

Table 2: Simulated mean observables for proton showers of energy 10^{15} eV at 0°. The errors given are the statistical errors of the mean values. Note that the position of the first interaction was fixed to the mean value for the respective model.

induced air showers are the main background in gamma ray experiments using the atmospheric Cherenkov technique and their simulated appearance depends on the hadronic interaction models. Small differences are seen in the lateral distributions (Fig. 4), resulting from the differing fractions of energy that is channeled into the electromagnetic (EM) component. This is visible in QGSJET option 2, where the biggest fraction of energy is going into the EM component, leading to the largest number of Cherenkov photons and lowest number of muons. SIBYLL and EPOS predict the largest numbers of Cherenkov photons, with about 7% more than the standard QGSJET option. This difference alone contributes 7% to the systematic energy error of proton showers in Cherenkov telescope experiments. The systematic shift is lower than the energy resolution of current instruments ($\approx$ 15% for 1 TeV photons), so it should not affect much measurements of the background in ACT instruments.

The ability to identify electromagnetic gamma ray showers from the overwhelming background of hadronic events directly determines the sensitivity of a Cherenkov telescope. It is based on the analysis of the shape of the shower image and depends on hadronic models, too. Hadronic showers produce more diffuse and larger images in the camera of a Cherenkov telescope than compact electromagnetic showers. Those hadron showers that are misidentified as gamma showers are usually characterised by a large fraction of the shower energy being dumped early on into the EM component [25].

The EM fraction in Fig. 4 looks similar to the inelasticity shown in Fig. 1, with values of about 1/3 of the ones of the inelasticity, as one would expect if 1/3 of the pions produced are π^0s. Again, most QGSJET variants produce a lower EM fraction than the standard QGSJET model, and SIBYLL and EPOS show different shapes. Overall, SIBYLL and EPOS were found to produce a larger EM fraction than QGSJET above 10^{12} eV. A larger EM fraction in the first interaction means a more photon-like appearance of the shower and a higher chance to misidentify a proton-induced shower as a gamma ray. Thus, all QGSJET variants give an equal or smaller rate of photon-like events than the QGSJET standard. Both, SIBYLL and EPOS will produce more gamma-like proton showers, but to quantify this would require full simulation of the telescope array and the reconstruction procedure.

This difference in the EM fraction can be partly explained by the differences in the inelasticity of the models, changing the amount of energy available for particle production. Once this was taken account of the QGSJET variants were found to give here a constant value of about 31% whereas SIBYLL is about 1% higher and EPOS 1% lower. As EPOS leaves more energy in secondary baryons, it is not surprising that the fraction in π^0s, and thus photons, is smaller.

4.2. Medium Energies (10^{15} eV)

At medium energies ($\sim 10^{15}$ eV) detector arrays usually measure shower particles arriving at ground level, with some arrays being able to distinguish between $e^{\pm}$, photons and muons. Therefore, Tab. 2 gives some typical shower observables for the different models. The left side of Fig. 5 shows differences in electron and muon numbers as function of core distance (lateral distributions) and ionisation energy deposit as a function of atmospheric depth (longitudinal distributions) for 10^{15} eV proton showers. At 10^{15} eV differences between the QGSJET model variations are less than $\pm$10% for electrons and muons at core distances of 10 to 1000 m. (The most relevant core distances at these energies are $\leq$ 200 m). The longitudinal distributions show very good agreement around the shower maximum ($\sim$550 g/cm^2) and differences up to $\pm$10% at ground level (here, 860 g/cm^2). SIBYLL lies well within the spread of the QGSJET options, but EPOS shows much flatter lateral distributions, for both electrons and muons, with many more particles large distances from the shower core and overall about 20% more muons. At ground level EPOS has 15% fewer electrons and 15% more muons than the reference model. Consequently, all energy assignments would be different on the 15-20% level and composition analysis were greatly affected

ACCEPTED MANUSCRIPT

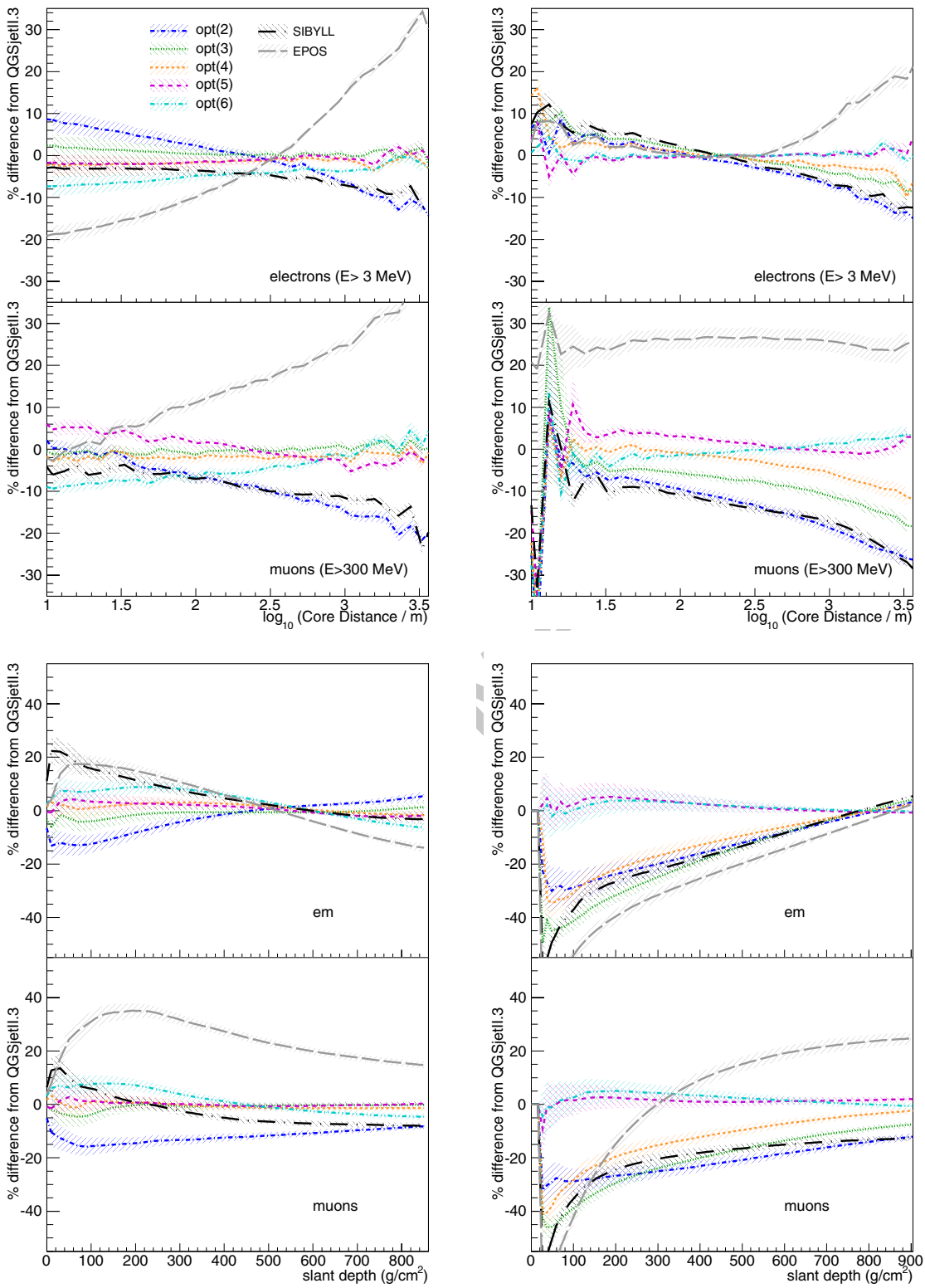

Figure 5: **Top:** Average percentage difference (compared to standard QGSJET-II) of the particle number N as function of the core distance at ground level (i.e. $N_i/N_{\mathrm{std}} - 1$) for electrons and muons. **Bottom:** Average percentage difference (compared to standard QGSJET-II) of the ionisation energy deposit as a function of the atmospheric depth for the em component and for muons. **Left:** 300 vertical proton showers of 10^{15} eV. **Right:** 100 proton showers at 20° with 10^{19} eV. Shaded error bands show statistical errors of the mean values.

ACCEPTED MANUSCRIPT

Model	S_{1000} (GeV)	$t_{1/2}$ (ns)	$X_{\max}$ (g/cm^2)	$N_{\max}(10^7)$
QGSJET-II (1)	10.01 ± 0.09	373.2 ± 1.4	773 ± 6	647 ± 2
QGSJET-II (2)	8.86 ± 0.11	385.7 ± 1.7	801 ± 6	642 ± 2
QGSJET-II (3)	9.38 ± 0.09	382.2 ± 1.4	803 ± 6	645 ± 2
QGSJET-II (4)	9.68 ± 0.10	378.9 ± 1.4	794 ± 5	645 ± 2
QGSJET-II (5)	10.01 ± 0.08	371.6 ± 1.4	780 ± 6	644 ± 2
QGSJET-II (6)	10.07 ± 0.10	372.9 ± 1.3	784 ± 5	648 ± 2
SIBYLL 2.1	9.00 ± 0.09	388.0 ± 1.7	795 ± 5	651 ± 2
EPOS 1.99	11.61 ± 0.18	368.9 ± 2.0	804 ± 5	630 ± 2

Table 3: Simulated mean observables for proton showers of energy 10^{19} eV at 20°. The errors are the statistical errors of the mean values. Note that the position of the first interaction was fixed to the mean value for the respective model.

by these differences. They are big enough for the KASCADE experiment to tell the difference. Indeed, there is evidence from KASCADE data [26] that the primary proton spectrum agrees better with direct measurements when QGSJET and SIBYLL are used for the analysis, than when EPOS is used.

The lateral distribution of QGSJET option 2 (enhanced diffraction) is very similar to that of SIBYLL at both 10^{15} and 10^{19} eV, suggesting that one of the major differences between the two models is the rate of diffraction. However differences can be seen between option 2 and SIBYLL in the results of single particle interactions, indicating that there are other important physical distinctions.

4.3. Ultra High Energies (10^{19} eV)

At 10^{19} eV the detector arrays must be sparse and no longer the total particle number is measured, but the particle density as a function of distance from the core. The energy is then determined from the density at some distance [27]. The time structure of the shower front, measured in the array detectors, carries information on the shower development and the primary mass. With fluorescence telescopes the longitudinal profile and the position of the shower maximum can be directly measured, from which the energy and the composition can be inferred. Commonly used observables at 10^{19} eV are listed in Tab. 3.

As expected, the deviations from standard QGSJET are largest at this energy, as the extrapolations of model parameters from collider energies are largest. Deviations in the lateral distributions of electrons and photons are less than +10% within 1000 m from the shower axis. For muons the variations within the QGSJET models are less than 20% at 1 km core distance, but all the options produce always smaller muon numbers than the standard QGSJET. SIBYLL gives almost the same results for electron and muon lateral distributions as QGSJET option 2, the version with the enhanced proton diffraction. Again, EPOS is distinctly different, with 25% more muons at ground level for all core distances. The QGSJET and SIBYLL muon numbers at ground are within 0 to -15% of the standard version. The EPOS electron numbers at ground are similar to those of the other models, owing to the fact that for the angle chosen the shower maximum is close to the ground. For more inclined showers larger differences would occur.

In the longitudinal distributions, the QGSJET options 2, 3 and 4 and SIBYLL have markedly lower particle numbers and energy deposits (40-20%) in the upper part of the shower than the standard. EPOS shows a similar trend, again developing slowly early in the shower, but quickly producing larger numbers of muons, with almost 30% more muons at ground level.

To reproduce data from experiments directly measuring muon numbers such as KASCADE and HiRes-MIA and from the Pierre Auger Observatory, where the muon content can be inferred indirectly [28], more muons in simulations seem to be required. EPOS seems to address the muon deficit problem, but would introduce a significantly different energy scale.

Significant differences are also seen in S_{1000}, a common observable used for the energy reconstruction in the 10^{19} eV region (see Tab. 3). The energy reconstruction based on option 2 would give ∼10% higher cosmic ray energies than the one using the standard QGSJET option, while EPOS would give 16% smaller energies. The differences in average $X_{\max}$ for the QGSJET models are less than 30 g/cm^2 (4%), with all the models producing deeper $X_{\max}$ values than standard QGSJET. The differences in $t_{1/2}$, which is used for composition analysis, are less than 5%, with SIBYLL and EPOS giving the extreme values.

5. Conclusion

The analysis of shower simulations demonstrates the increase in systematic uncertainties (introduced by variation of model parameters) as the primary particle energy increases, and with it the extrapolation of the models. Our study indicates that parameter variations within one model generally cannot reproduce

ACCEPTED MANUSCRIPT

the full variance possible between models. None of the parameter variations investigated in QGSJET was able to mimic the behaviour of the EPOS model: At any energy, EPOS has far more muons than all other models and specifically than the QGSJET standard version. Differences in several observables amount to $< 10\%$ in the TeV range and to 20-30% in the PeV and EeV ranges, causing sizeable systematic errors on the energy scale and composition analysis. Within QGSJET, at all primary energies the largest effects are observed due to the increase of the rate of diffraction for protons and pions, making diffraction the feature with the largest impact on the overall development of the shower.

EPOS is a relatively new model and still has to prove its qualities by being compared in detail to results from different (past and present) experiments from TeV to EeV energies.

The lateral and longitudinal distribution pattern of the electromagnetic and muonic components in air showers shows complex variations between models, which depend on the energy and the level of shower development, the zenith angle, etc. Therefore, complete simulations of showers, detectors and analysis procedures, using different interaction models are needed for a meaningful data analysis. The model uncertainties at high energies are of a size that makes analysis of nuclear composition at $\geq$EeV energies rather difficult (with the observables considered here), as differences between proton and iron induced showers are not much larger than the uncertainties due to the models. On the other hand, the uncertainties are large enough that current experiments are able to tell which model fits best. Also, new data from LHC and RHIC do increasingly constrain the models, and help to make the extrapolation to highest energies more reliable. But ultimately, only a coherent description of cosmic ray phenomena and hadronic interaction physics over the full energy range will be a convincing proof of the correct interpretation of cosmic ray data.

Acknowledgments

SO acknowledges the support by the program Romforskning of Norsk Forsknigsradet.

[1] V.N. Gribov, Sov. Phys. JETP 26 (1968) 414

[2] R.J. Glauber, G. Matthiae, Nucl. Phys. B 21 (1970) 135

[3] V.N. Gribov, Sov2. Phys. JETP 29 (1969) 483

[4] R. Ulrich, R. Engel and M. Unger, arXiv:1010.4310 [hep-ph]

[5] S. Ostapchenko, Phys. Rev. D 74 (2006) 014026 and
AIP Conf. Proc. 928 (2007) 118

[6] R.S. Fletcher et al., Phys. Rev. D 50 (1994) 5710
E.J. Ahn et al., Phys. Rev. D 80 (2009) 094003

[7] K. Werner et al., Phys. Rev. C 74 (2006) 044902

[8] M. Hladik et al., Phys. Rev. Lett. 86 (2001) 3506

[9] T. Pierog and K. Werner, Phys. Rev. Lett. 101 (2008) 171101

[10] D. Heck et al., Report FZKA 6019 (1998), Forschungszentrum Karlsruhe

[11] M.L. Good and W.D. Walker, Phys. Rev. 120 (1960) 1857

[12] A.B. Kaidalov, Phys. Rep. 50 (1979) 157

[13] D. Kharzeev, Phys. Lett. B 378 (1996) 238

[14] D. d'Enterria et al., arXiv:1101.5596v2 [astro-ph.HE]

[15] A. Tricomi for the LHCf Collaboration, Talk at 35th ICHEP, Paris (2010)
Early Physics with the LHCf detector at LHC
http://indico.cern.ch/contributionDisplay.py?contribId=860&confId=73513

[16] J.A. Hinton, New Astronomy Review 48 (2004) 331

[17] T.C. Weekes et al., Astrop. Phys. 17 (2002) 221

[18] E. Lorenz, New Astronomy Review 48 (2004) 339

ACCEPTED MANUSCRIPT

[19] T. Antoni et al. (KASCADE Collaboration), Nucl. Instr. Meth. A 513 (2003) 490

[20] Z. Cao et al. (LHAASO Collaboration), Proc. 31st ICRC (2009), Łódź, Poland
http://icrc2009.uni.lodz.pl/

[21] J.N. Matthews et al. (Telescope Array Collaboration), Proc. 31st ICRC (2009), Łódź, Poland
http://icrc2009.uni.lodz.pl/

[22] J. Abraham et al. (Pierre Auger Collaboration), Nucl. Instr. Meth. A 523 (2004) 50

[23] J. Abraham et al. (Pierre Auger Collaboration), Phys. Rev. Lett. 101 (2008) 061101

[24] J. Abraham et al. (Pierre Auger Collaboration), Astrop. Phys. 29 (2008) 243-256

[25] G. Maier, J. Knapp, Astrop. Phys. 28 (2007) 72

[26] A. Haungs for the KASCADE-Grande Collaboration, Talk at ARENA Meeting, Nantes (2010)
Latest results and perspectives of the KASCADE-Grande EAS facility
http://indico.in2p3.fr/contributionDisplay.py?contribId=17&confId=2719

[27] D. Newton et al., Astrop. Phys. 26 (2007) 414

[28] F. Schmidt et al., Astrop. Phys. 29 (2008) 355

ACCEPTED MANUSCRIPT